

SUPPORTING INFORMATION

Yellow to greenish-blue colour-tunable photoluminescence and 4f-centered slow magnetic relaxation in cyanido-bridged Dy^{III}(4-hydroxypyridine) – Co^{III} layered material

Szymon Chorazy,^{*a,b} Junhao Wang,^a and Shin-ichi Ohkoshi^{*a}

^aDepartment of Chemistry, School of Science, The University of Tokyo, 7-3-1 Hongo, Bunkyo-ku, Tokyo, 113-0033, Japan.

^bFaculty of Chemistry, Jagiellonian University, Ingardena 3, 30-060 Krakow, Poland.

*Corresponding authors: ohkoshi@chem.s.u-tokyo.ac.jp; chorazy@chemia.uj.edu.pl

Experimental details.	S2
Infrared absorption spectrum of 1 compared with the spectrum of 4-hydroxypyridine. (Figure S1)	S5
Thermogravimetric analysis of 1 . (Figure S2)	S6
Crystal data and structure refinement of 1 . (Table S1)	S7
Detailed structure parameters of 1 . (Table S2)	S8
Results of Continuous Shape Measure Analysis for [Dy ^{III} (NC) ₃ (4-OHpy) ₂ (H ₂ O) ₃] complexes in 1 . (Table S3)	S9
Detailed insight into the geometry of [Dy ^{III} (NC) ₃ (4-OHpy) ₂ (H ₂ O) ₃] complexes in 1 . (Figure S3)	S9
Spatial arrangement of cyanido-bridged layers of 1 within the <i>bc</i> , <i>ac</i> , and <i>ab</i> crystallographic planes. (Figure S4)	S10
The views of the supramolecular network in 1 involving the non-covalent interactions of the intralayer and interlayer character. (Figure S5)	S11
Experimental powder X-ray diffraction patterns of 1 , and its magnetically diluted sample, 1md , compared with the calculated pattern based on the single-crystal XRD structural model of 1 . (Figure S6)	S12
Solid state UV-Vis-NIR absorption spectra of 1 compared with the relevant spectra of 4-OHpy and K ₃ [Co(CN) ₆]. (Figure S7)	S13
Analysis of solid state UV-Vis-NIR absorption spectrum of 1 compared with the analyses of the relevant spectra of 4-OHpy and K ₃ [Co ^{III} (CN) ₆]. (Table S4)	S14
Solid state UV-Vis emission and excitation spectra of free 4-OHpy, together with the related emission colour presented on the CIE 1931 chromaticity diagram. (Figure S8)	S15
Room temperature and low temperature solid state UV-Vis emission spectra of 1 under various excitation wavelengths, together with the emission colours presented on the CIE 1931 chromaticity diagrams, and the related excitation spectra for the emission peaks of 4-OHpy and Dy ^{III} . (Figure S9)	S16
Summary of <i>xy</i> parameters of the CIE 1931 chromaticity scale for the emission colours of 1 detected at room and low temperature at various indicated wavelength of the excitation light. (Table S5)	S17
Frequency dependences of in-plane χ_M' and out-of-plane χ_M'' magnetic susceptibilities of 1 under <i>ac</i> magnetic field of 3 Oe at <i>T</i> = 1.9 K, and various indicated <i>dc</i> magnetic fields. (Figure S10)	S18
Full <i>ac</i> magnetic characteristics of 1 under <i>H</i> _{dc} = 1000 Oe and <i>H</i> _{ac} = 3 Oe. (Figure S11)	S18
Parameters obtained by fitting the Argand χ_M'' - χ_M' plots of 1 using the generalized Debye model. (Table S6)	S19
Direct-current (<i>dc</i>) magnetic properties of 1md : temperature dependence of $\chi_M T$ at <i>H</i> _{dc} = 1000 Oe, and the field dependence of molar magnetization, <i>M</i> at <i>T</i> = 1.8 K. (Figure S12)	S20
Frequency dependences of in-plane χ_M' and out-of-plane χ_M'' magnetic susceptibilities of 1md under <i>ac</i> magnetic field of 3 Oe at <i>T</i> = 1.9 K, and various indicated <i>dc</i> magnetic fields. (Figure S13)	S21
Full <i>ac</i> magnetic characteristics of 1md under <i>H</i> _{dc} = 500 Oe and <i>H</i> _{ac} = 3 Oe. (Figure S14)	S21
Parameters obtained by fitting the Argand χ_M'' - χ_M' plots of 1md using the generalized Debye model. (Table S7)	S22
References to Supporting Information.	S23

Experimental details.

Materials

Dysprosium(III) chloride hexahydrate ($\text{Dy}^{\text{III}}\text{Cl}_3 \cdot 6\text{H}_2\text{O}$, CAS: 15059-52-6, Wako Pure Chemicals Industries, Ltd.), yttrium(III) chloride hexahydrate ($\text{Y}^{\text{III}}\text{Cl}_3 \cdot 6\text{H}_2\text{O}$, CAS: 10025-94-2, Wako Pure Chemicals Industries, Ltd.), 4-hydroxypyridine (4-OHpy, 4-pyridinol, CAS: 626-64-2, Sigma-Aldrich), and potassium hexacyanidocobaltate(III) ($\text{K}_3[\text{Co}^{\text{III}}(\text{CN})_6]$, CAS: 13963-58-1, Sigma-Aldrich) were purchased from commercial sources, and used without further purification.

Synthesis and basic characterization of **1**

The 0.24 mmol (80.0 mg) portion of $\text{K}_3[\text{Co}^{\text{III}}(\text{CN})_6]$ was dissolved in the 0.7 mL of distilled water to get solution I. Then, the 0.24 mmol (90.0 mg) portion of $\text{Dy}^{\text{III}}\text{Cl}_3 \cdot 6\text{H}_2\text{O}$, and the 0.48 mmol (46.0 mg) portion of 4-hydroxypyridine (4-OHpy) were dissolved together in the 0.7 mL of distilled water. The resulting suspension was stirred with continuous heating up to the boiling point to obtain the yellowish transparent solution II. Then, the hot solution II was quickly poured into the solution I which was followed by a suction filtration after stirring the mixed solution for several seconds. The yellowish clear filtrate was left undisturbed for crystallization. The colorless elongated plate-shaped crystals of **1** started to appear after a few minutes. The whole crystalline product was collected by a suction filtration after one day. The crystals were washed by a small portion of cold distilled water and ethanol, and air-dried for 4 hours. The resulting crystalline material was air-stable and could be identified by the composition of $\{[\text{Dy}^{\text{III}}(4\text{-OHpy})_2(\text{H}_2\text{O})_3][\text{Co}^{\text{III}}(\text{CN})_6]\} \cdot 0.5\text{H}_2\text{O}$ (**1**) as determined by the CHN elemental analysis, supported by IR spectrum (Figure S1), and thermogravimetric studies (Figure S2). Yield: 80 mg, 53 %. In order to obtain a single crystal sufficiently large for monocrystalline X-ray diffraction measurement, **1** was prepared by a similar strategy except that the concentrations of precursors (solution I and II) were decreased. The optimized conditions consist of the 0.24 mmol (40.0 mg) portion of $\text{K}_3[\text{Co}^{\text{III}}(\text{CN})_6]$ dissolved in the 0.5 mL of distilled water, and the 0.12 mmol (54.5 mg) portion of $\text{Dy}^{\text{III}}(\text{NO}_3)_3 \cdot 6\text{H}_2\text{O}$ with the 0.24 mmol (23.0 mg) portion of 4-OHpy dissolved together in 0.5 mL of distilled water. The obtained single crystals were isostructural to those obtained by the original method, which was confirmed by the powder X-ray diffraction experiment (Figure S6).

IR spectrum (KBr, cm^{-1} , Figure S1). CN^- stretching vibrations: 2181vs, 2167vs, 2154vs, 2135vs, indicated the presence of both bridging and terminal modes as the splitting of the peak with characteristic shifts towards higher energies are observed when compared with the $\nu(\text{CN})$ of 2129vs for $\text{K}_3[\text{Co}^{\text{III}}(\text{CN})_6]$.^{S1} Other peaks: 3609s, 3522s, 3264s, 3155s, br, OH hydrogen bonding; 1639 m $\delta(\text{H}_2\text{O})$; 1590m, 1545vs, 1389s, 999s, C=C, C=N stretching mode; 1521vs C=O stretching mode due to isomerization; 1283vw, 1246vw, 1188s, 873w, 859w, C-H and ring deformation. All these peaks can be found in pure 4-hydroxypyridine (4-OHpy), but their positions are variously shifted in **1** indicating the coordination of 4-OHpy by Dy^{III} .

CHN elemental analysis. Anal. Calcd. for $\text{Co}_1\text{Dy}_1\text{C}_{16}\text{H}_{17}\text{N}_8\text{O}_{5.5}$ ($M_w = 630.8 \text{ g}\cdot\text{mol}^{-1}$): C, 30.5%; H, 2.7%; N, 17.8%. Found: C, 30.2%; H, 2.8%; N, 18.0%. TGA (Figure S2): loss of 0.5 H_2O (crystallization solvent, non-coordinated), calcd. 1.4%, found 1.4%; loss of 3 H_2O (coordinated), calcd. 8.6%, found, 8.5%.

Crystal structure determination of **1**

Single crystal X-ray diffraction analysis of **1** was performed using a Rigaku R-AXIS RAPID imaging plate area detector with graphite monochromated Mo K α radiation. The single crystal was dispersed in a paratone-N oil, mounted on Micro MountsTM holder, and measured at the low temperature of 100(2) K. The crystal structure was solved by a direct method using SHELXS-97, and refined using a full-matrix least squares technique of SHELXL-2014/7.^{S2} Calculations were executed using partially Crystal Structure crystallographic software package, and partially WinGX (ver. 1.80.05) integrated system. All non-hydrogen atoms were refined anisotropically. The hydrogen atoms were found from the electron density map, and refined isotropically, however the part of O-H distances were fixed by the DFIX command in order to stabilize their positions during the refinement procedure. The part of C and N atoms of cyanides, and O atom of one coordinated water molecule, reveal structural disorder affecting the refinement procedure, and the shapes of their thermal ellipsoids. Thus, the restraints on their thermal ellipsoids (DELU, ISOR, SIMU) were applied. The hydrogen atom of the hydroxyl group of 4-OHpy and the crystallization water molecule, which presence was indicated by the elemental analysis and thermogravimetry, could not be located due to their probable significant structural disorder leading to the multiple possible positions with only partial occupancies. Structural diagrams were prepared using Mercury 3.5.1 programme. CCDC reference number for the crystal structure of **1** is 1477277. The details of the crystal structure and structure refinement were gathered in Table S1, while the selected detailed structure parameters are presented in Table S2.

Synthesis and characterization of magnetically diluted sample of **1**, **1md**

In order to enhance the magnetic relaxation processes occurring for Dy^{III} complexes, the magnetically diluted sample of **1** with the partial replacement of paramagnetic Dy^{III} by diamagnetic Y^{III} centers was prepared. Such magnetically diluted sample, named **1md**, was obtained by the modification of the synthetic procedure described for **1**. The 0.48 mmol (160.0 mg) portion of K₃[Co^{III}(CN)₆] was dissolved in the 1.5 mL of distilled water to get solution I. Then, the 0.05 mmol (18.8 mg) portion of Dy^{III}Cl₃·6H₂O, the 0.43 mmol (130.5 mg) portion of Y^{III}Cl₃·6H₂O, and the 0.96 mmol (92.0 mg) portion of 4-hydroxy-pyridine (4-OHpy) were dissolved together in the 1.5 mL of distilled water. The resulting suspension was mixed with heating up to the boiling point which gave the light yellow solution II. Then, the hot solution II was added to the solution I, and the mixture was filtrated. The clear filtrate was left undisturbed for crystallization. The colorless platelet crystals of **1md** appeared immediately. They were collected by a suction filtration after one day, washed by cold water and ethanol, and dried on the air for 4 hours. Yield: 135 mg, 49 %. The composition of **1md**, precisely investigated by the CHN elemental analysis of the standard microanalytical method, and the metal analysis executed by means of inductively coupled plasma mass spectrometry (ICP-MS) technique, was found to be analogous to the composition of **1** with the partial replacement of Dy by Y, that is {[Dy^{III}_{0.18}Y^{III}_{0.82}(4-OHpy)₂(H₂O)₃][Co^{III}(CN)₆]}·0.5H₂O (**1md**). As a result, **1md**, contains 18% of Dy and 82% of Y, considering the f-metal composition, thus, **1md** can be treated as the magnetically diluted sample of **1**. **1md** is isostructural with **1** as was confirmed by the identical IR spectra, and, more precisely, by the powder X-ray diffraction studies showing the identical PXRD patterns for both the polycrystalline samples of **1** and **1md**, and the pattern simulated from the single-crystal X-ray diffraction model of **1** (Figure S6).

IR spectrum (KBr, cm^{-1}). CN⁻ stretching vibrations: 2182vs, 21687vs, 2154vs, 2135vs, indicated the presence of both bridging and terminal modes of cyanides, with peaks situated at the similar positions as observed in **1** (see above). Other peaks: 3610s, 3524s, 3264s, 3151s, br, OH hydrogen bonding; 1639 m $\delta(\text{H}_2\text{O})$; 1590m, 1545vs, 1390s, 999s, C=C, C=N stretching mode; 1521vs C=O stretching mode due to isomerization; 1283vw, 1245vw, 1188s, 874w, 859w, C-H and ring deformation. All these peaks can be found in pure 4-hydroxypyridine (4-OHpy), but their positions are variously shifted, similarly to found in **1**.

CHN and ICP-MS elemental analysis. Anal. Calcd. for $\text{Co}_1\text{Dy}_{0.18}\text{Y}_{0.82}\text{C}_{16}\text{H}_{17}\text{N}_8\text{O}_{5.5}$ ($M_w = 570.5 \text{ g}\cdot\text{mol}^{-1}$): Co, 10.3% Dy, 5.1%; Y, 12.8%, C, 33.7%; H, 3.0%; N, 19.7%. Found: Co, 10.3%; Dy, 5.3%; Y, 13.1%; C, 33.7%; H, 3.0%; N, 20.0%.

Physical techniques

Infrared absorption spectra were collected using JASCO FTIR-4100 spectrometer in the 500–4000 cm^{-1} range on the polycrystalline samples grinded and pressed with potassium bromide. Elemental analysis of metals (Dy, Y, Co) was performed using Agilent 7700 ICP-MS. Thermogravimetric analysis was performed using a Rigaku Thermo Plus TG8120 apparatus in the 20–400°C range under an air atmosphere with a heating rate of 1 °C, with aluminium oxide used as a reference. UV-Vis-NIR diffuse reflectance spectra were measured using a JASCO V-670 spectrophotometer on the polycrystalline samples mixed with barium sulfate. Powder X-ray diffraction pattern of the polycrystalline sample of **1** was collected on a Rigaku Ultima-IV equipped with $\text{CuK}\alpha$ radiation ($\lambda = 1.5418 \text{ \AA}$). Emission and excitation spectra were gathered on a Horiba Jobin-Yvon Fluorolog®-3 (FL3-211) spectrofluorimeter (model TKN-7) equipped with an Xe (450 W) lamp as an excitation source, and the room temperature R928P emission detector working in a photon-counting mode. The collection and analysis of the emission and excitation spectra were performed using a Fluorescence® software. The measurements were executed at room temperature in the standard solid state holder, and at low temperature of 77 K in the optical cryostat cooled by liquid nitrogen. Magnetic measurements were performed using a Quantum Design MPMS XL magnetometer on the polycrystalline sample submerged in a paraffin oil to avoid the rotation of crystals under an applied magnetic field.

Calculations

Continuous Shape Measure Analysis for the determination of the geometry of eight-coordinated Dy^{III} complexes in **1** was performed using SHAPE software ver. 2.1.^{S3}

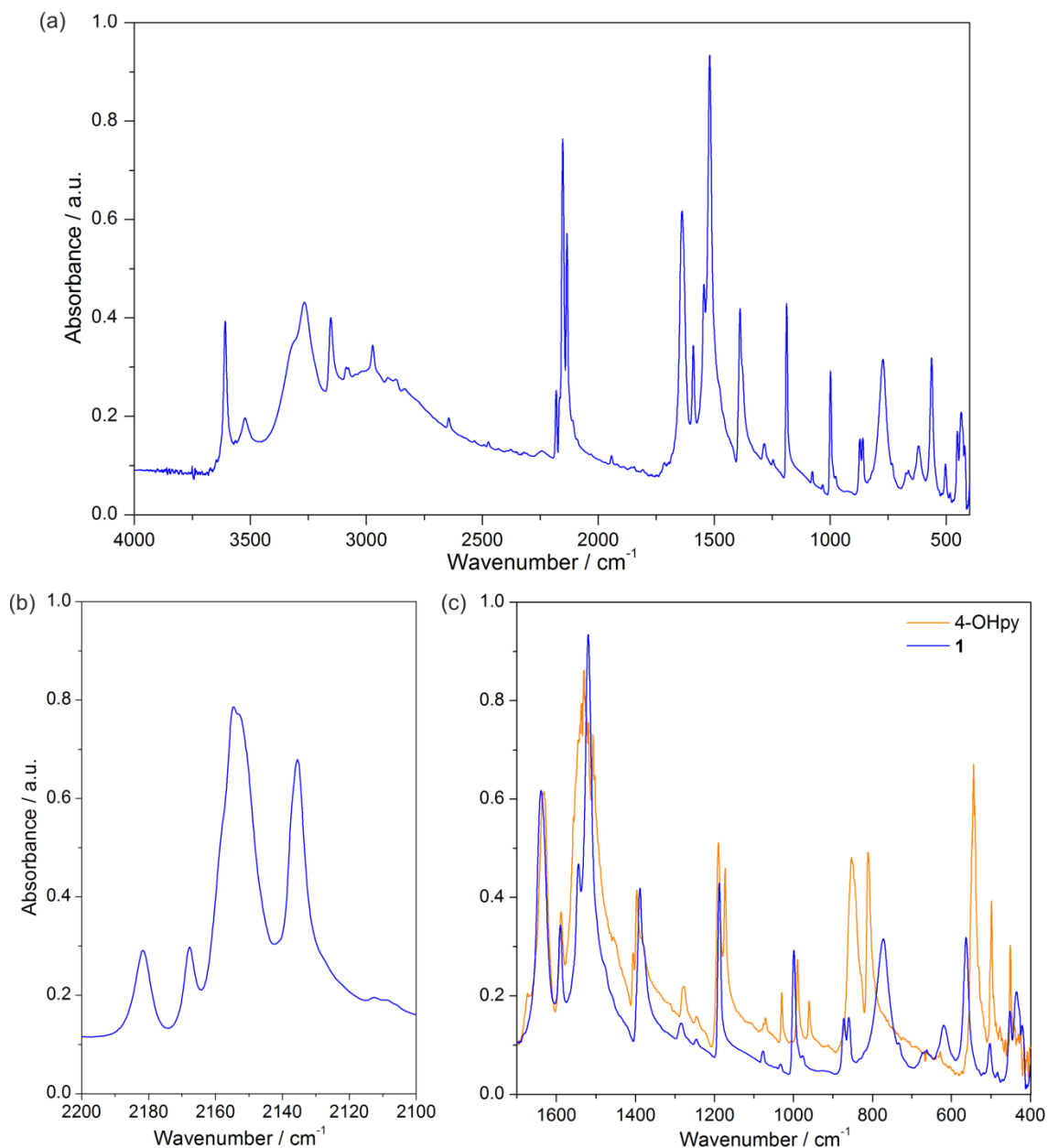


Figure S1. Infrared absorption spectrum of **1** (blue line) compared with the spectrum of 4-hydroxypyridine (orange line) in the various wavenumber ranges: (a) in the full 4000–400 cm⁻¹ range, (b) in the 2200–2100 cm⁻¹ range of the stretching vibrations of cyanides, and (c) in the 1700–400 cm⁻¹ range dominated by vibrations within the organic part. The comparison with pure 4-OHpy ligand is only presented in (c) where the organic ligand shows the very characteristic absorption peaks.

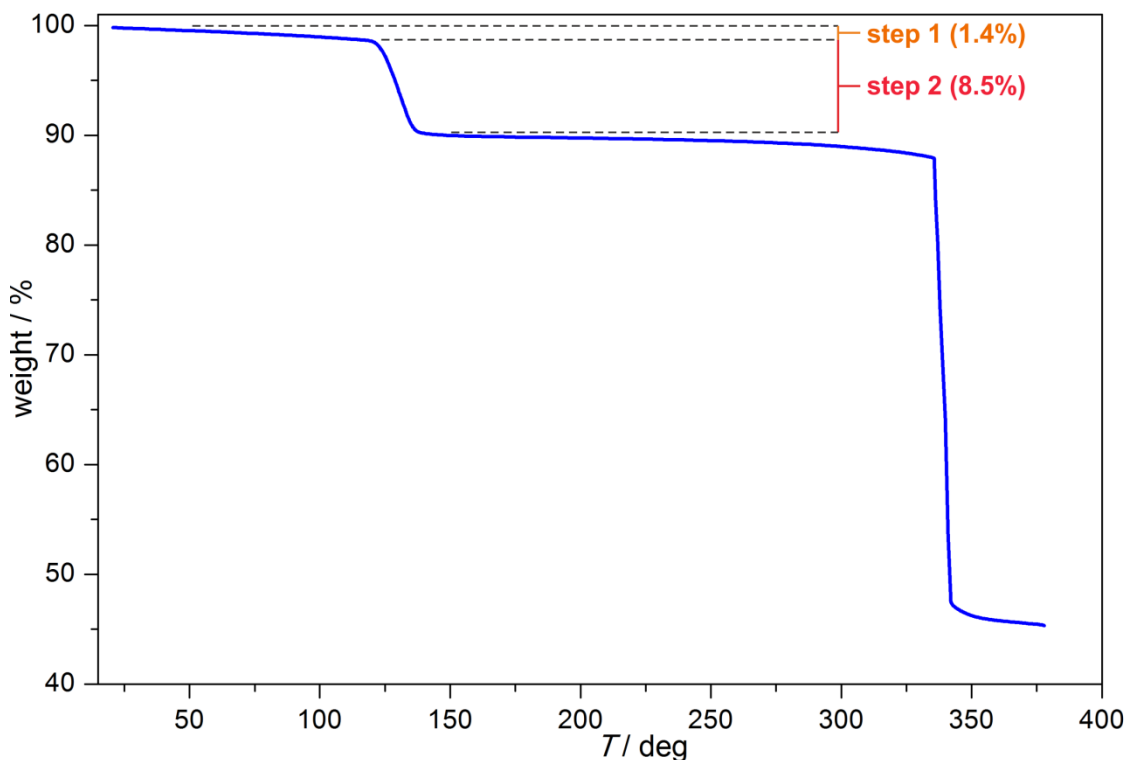


Figure S2. Thermogravimetric curve of **1** measured under an air atmosphere in the 20–400 °C temperature range with the two indicated steps related to loss of water molecules (see comment below).

Comment to Figure S2:

On heating from room temperature to ca. 120°C, **1** reveals a continuous decrease of the mass from 100% to 98.6% (step 1, Figure S2). The related weight loss of 1.4% can be explained by the removal of weakly bonded, non-coordinated water molecules in the amount of 0.5 molecule per one {Dy^{III}Co^{III}} unit (calculated weight loss of 1.4%). On further heating, the abrupt decrease of the mass from 98.6% to 90.1% in the narrow range of 120–135°C is observed (step 2, Figure S2). This weight loss by the value of 8.5% corresponds nicely to the removal of three coordinated water molecules per one {Dy^{III}Co^{III}} unit (calculated weight loss of 8.6%). Thus, the two indicated steps in the TGA curve confirms the composition of **1**, {[Dy^{III}(4-OHpy)₂(H₂O)₃][Co^{III}(CN)₆]}·0.5H₂O, determined by the CHN elemental analysis. The dehydrated phase of the presumable formula {[Dy^{III}(4-OHpy)₂][Co^{III}(CN)₆]}, seems to be quite stable as above 135°C a long plateau is observed almost up to 340°C. At the highest temperatures, the mass of **1** dramatically decreases reaching only 45 % of the starting value at 375°C.

Table S1. Crystal data and structure refinement for **1**

Compound		1
method		single-crystal XRD
formula		Dy ₁ Co ₁ C ₁₆ H ₁₆ N ₈ O ₅
formula weight [g·mol ⁻¹]		621.8
<i>T</i> [K]		100(2)
λ [Å]		0.71075 (Mo K α)
crystal system		monoclinic
space group		<i>P</i> 2 ₁ /m (no. 11)
unit cell	<i>a</i> [Å]	6.8970(5)
	<i>b</i> [Å]	15.6685(9)
	<i>c</i> [Å]	9.6096(6)
	α [deg]	90
	β [deg]	102.131(7)
	γ [deg]	90
<i>V</i> [Å ³]		1015.28(12)
<i>Z</i>		2
calculated density [g·cm ⁻³]		2.034
absorption coefficient [cm ⁻¹]		4.516
<i>F</i> (000)		602
crystal size [mm × mm × mm]		0.09 × 0.05 × 0.03
θ range [deg]		3.021 – 27.481
limiting indices		-8 < <i>h</i> < 8 -18 < <i>k</i> < 20 -11 < <i>l</i> < 12
collected reflections		9618
unique reflections		2407
<i>R</i> _{int}		0.0855
completeness [%]		99.8
max. and min. transmission		0.674 and 0.888
refinement method		full-matrix least-squares on <i>F</i> ²
data/restraints/parameters		2407/41/185
GOF on <i>F</i> ²		1.208
final <i>R</i> indices		<i>R</i> ₁ = 0.0624 [<i>I</i> > 2 σ (<i>I</i>)] <i>wR</i> ₂ = 0.1119 (all data)
largest diff peak and hole		2.934 and -2.729 e·Å ⁻³

Table S2. Detailed structure parameters of **1**

Details of [Co ^{III} (CN) ₆] ³⁻ complex		Details of [Dy ^{III} (4-OHpy) ₂ (H ₂ O) ₃ (NC) ₃] complex	
Parameter	Value [Å, °]	Parameter	Value [Å, °]
Co1-C1	1.918(14)	Dy1-O1	2.260(5)
Co1-C2	1.878(11)	Dy1-O2	2.378(6)
Co1-C3	1.910(11)	Dy1-O3	2.477(9)
Co1-C4	1.831(12)	Dy1-N1	2.520(11)
Co1-C5	1.905(8)	Dy1-N2	2.478(10)
C1-N1	1.105(16)	Dy1-N3	2.483(10)
C2-N2	1.143(14)	Dy1-N1-C1	154.1(11)
C3-N3	1.136(14)	Dy1-N2-C2	171.9(10)
C4-N4	1.177(14)	Dy1-N3-C3	158.7(10)
C5-N5	1.142(10)	Dy1-O1-C6	149.1(5)
Co1-C1-N1	174.1(12)	N1-Dy1-N2	69.2(3)
Co1-C2-N2	174.7(11)	N2-Dy1-N3	133.9(3)
Co1-C3-N3	173.6(11)	N3-Dy1-N1	156.9(4)
Co1-C4-N4	178.6(10)	O1-Dy1-O1	75.0(3)
Co1-C5-N5	177.2(8)	O1-Dy1-O2	73.9(2)
C1-Co1-C4	175.6(6)	O2-Dy1-O3	71.74(18)
C2-Co1-C3	175.0(5)	O3-Dy1-O2	71.74(18)
C5-Co1-C5	175.2(5)	O2-Dy1-O1	73.9(2)
C1-Co1-C2	87.6(5)	O1-Dy1-N1	79.8(3)
C1-Co1-C3	97.4(5)	O1-Dy1-N2	131.3(2)
C1-Co1-C5	91.2(2)	O1-Dy1-N3	81.9(3)
C2-Co1-C4	87.9(5)	O2-Dy1-N1	94.7(2)
C2-Co1-C5	88.0(3)	O2-Dy1-N2	72.33(18)
C3-Co1-C4	87.0(5)	O2-Dy1-N3	93.7(2)
C3-Co1-C5	91.9(3)	O3-Dy1-N1	133.8(3)
C4-Co1-C5	88.6(2)	O3-Dy1-N2	64.6(3)
Co1-Dy1 (C1N1)	5.356	O3-Dy1-N3	69.3(3)
Co1-Dy1 (C2N2)	5.470	4OHpy-4OHpy torsion between py rings	134.8
Co1-Dy1 (C3N3)	5.392		

Table S3. Results of Continuous Shape Measure Analysis for $[\text{Dy}^{\text{III}}(\text{NC})_3(4\text{-OHpy})_2(\text{H}_2\text{O})_3]$ complex in **1**

Dy complex	CSM parameters			Geometry
	BTP-8	SAPR-8	DD-8	
$[\text{Dy}^{\text{III}}(\text{NC})_3(4\text{-OHpy})_2(\text{H}_2\text{O})_3]$	2.708	3.268	0.544	DD-8

* CSM parameters:^[S3]

CSM BTP-8 = the parameter related to the bicapped trigonal prism geometry (C_{2v} symmetry)

CSM SAPR-8 = the parameter related to the square antiprism (D_{4d} symmetry)

CSM DD-8 = the parameter related to the dodecahedron (D_{2d} symmetry)

CSM = 0 for the ideal geometry and the increase of CSM parameter corresponds to the increasing distortion from the ideal polyhedron.

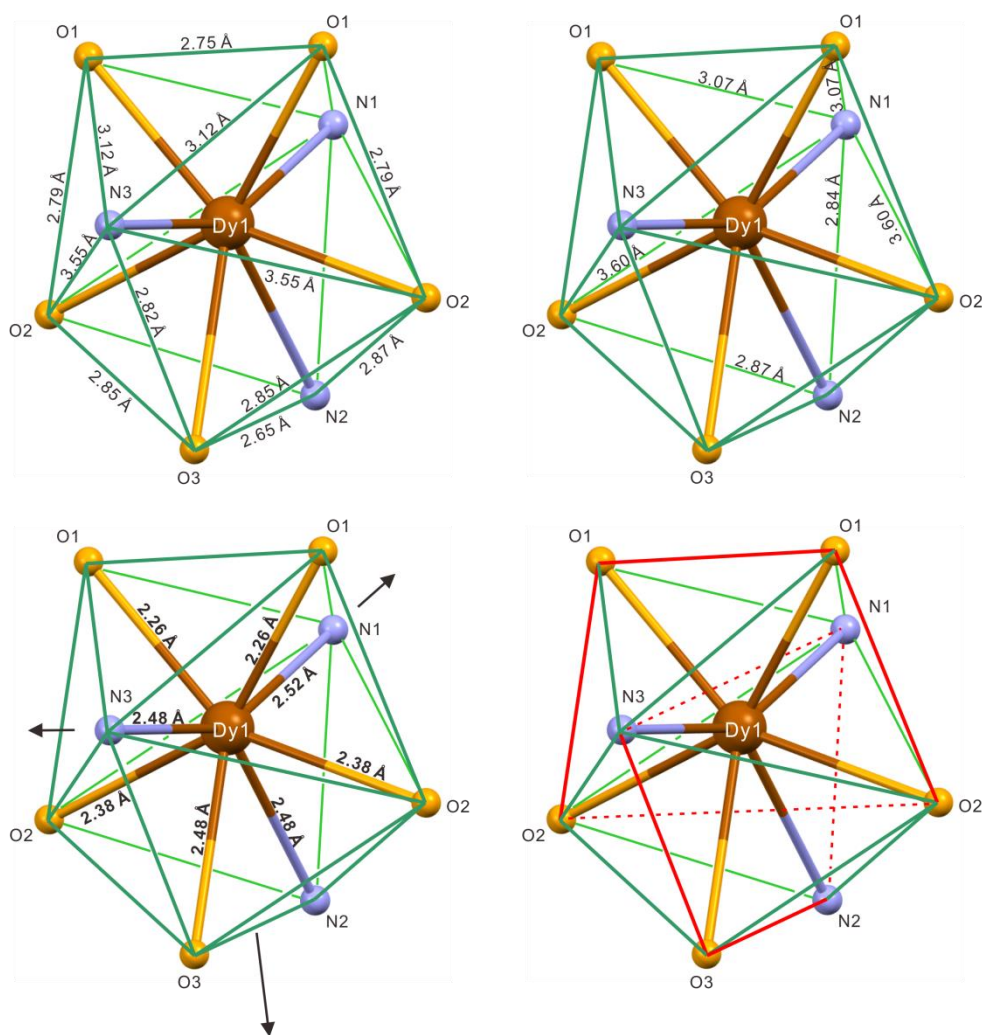


Figure S3. Detailed insight into the geometry of $[\text{Dy}^{\text{III}}(\text{NC})_3(4\text{-OHpy})_2(\text{H}_2\text{O})_3]$ complexes in **1**: the detailed dimensions of the coordination polyhedron of the distorted DD-8 geometry (top), the arrangement of bond lengths within the polyhedron with the indicated elongation directions (black arrows, bottom, left), and the visualization of the DD-8 character of the coordination polyhedron that is the perpendicular alignment of two trapezoids (red lines, bottom, right).

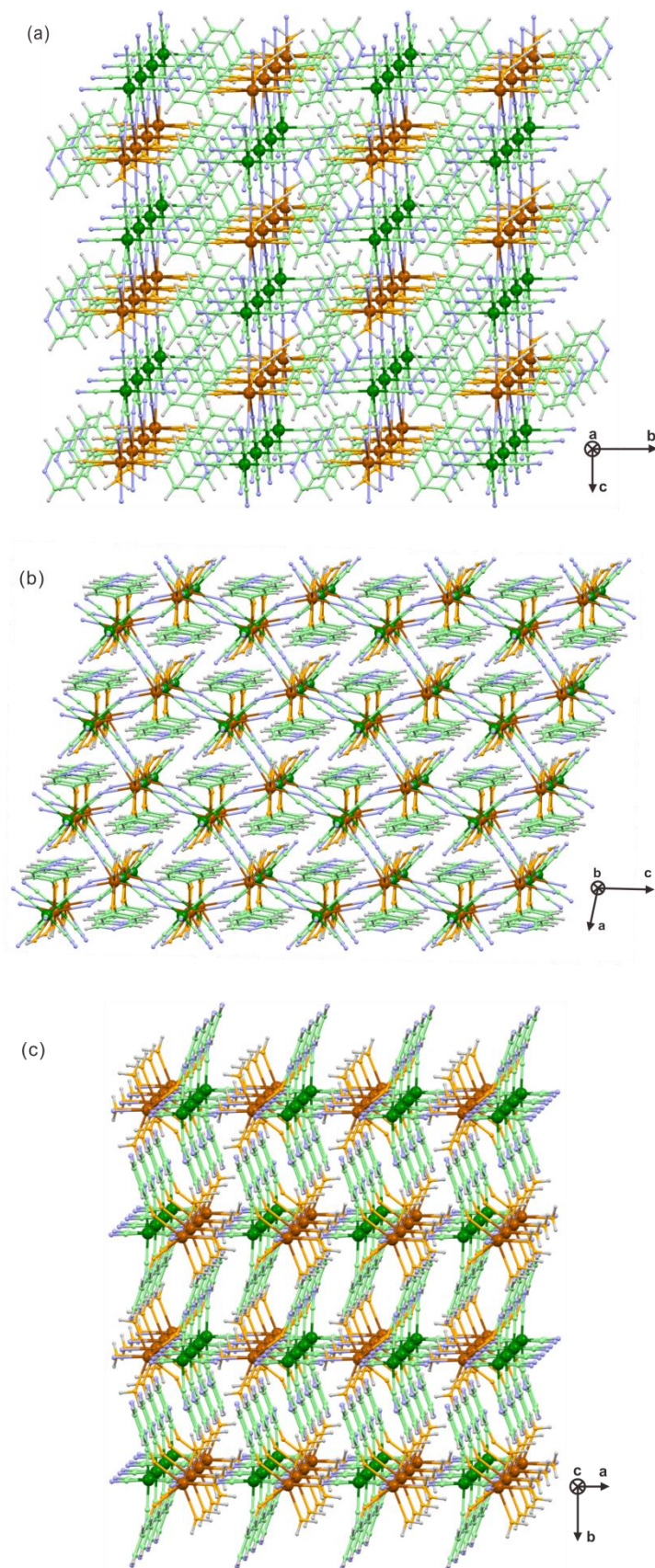


Figure S4. The views of the spatial arrangement of cyanido-bridged layers of **1** within the *bc* (a), *ac* (b), and *ab* (c) crystallographic planes. Colours: Dy, brown; Co, dark green; C, light green; N, light blue; O, orange; hydrogen, light grey.

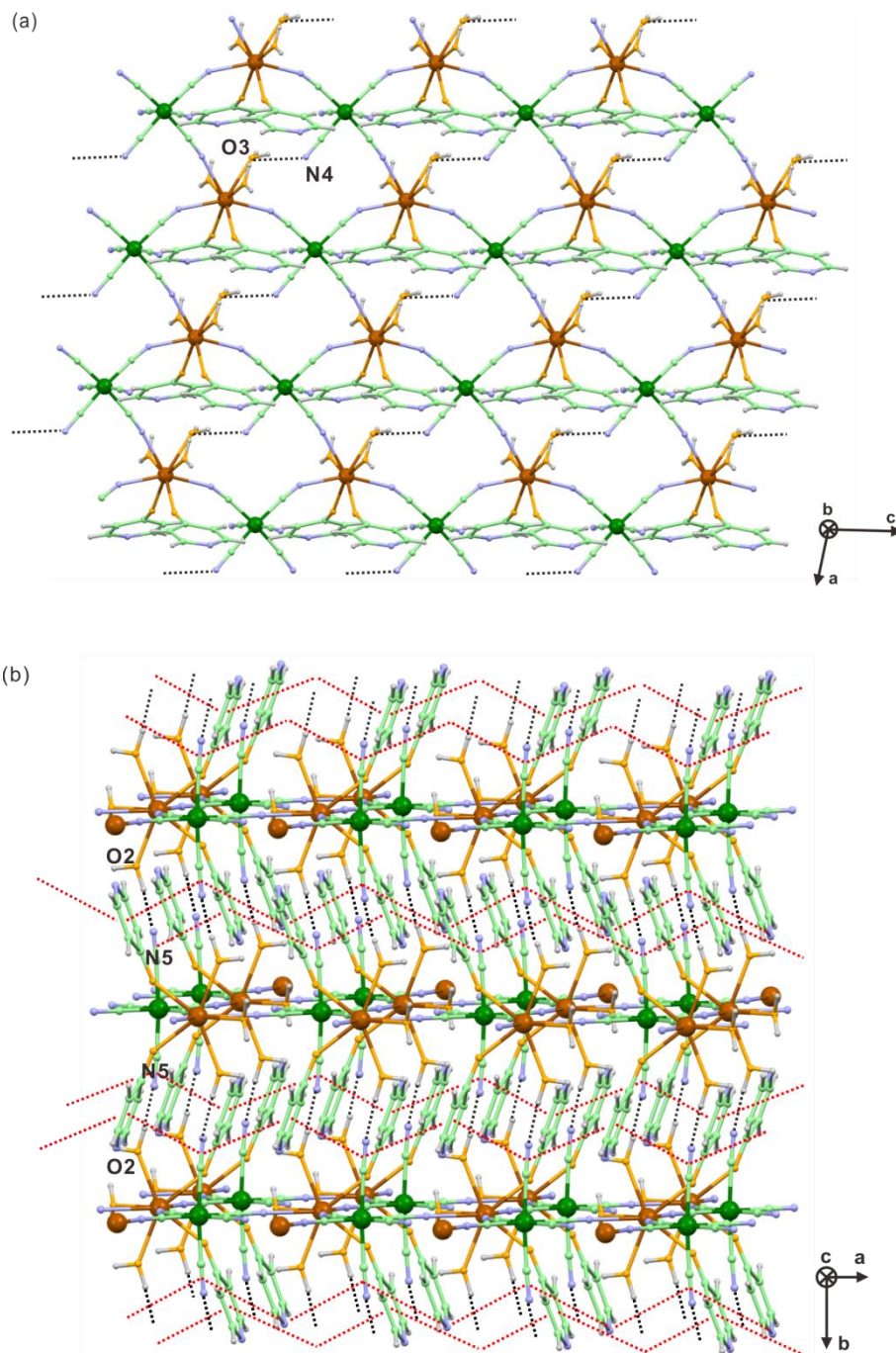


Figure S5. The views of the supramolecular network in **1** involving the non-covalent interactions of the intralayer (a), and interlayer (b) character. The hydrogen bonds between water molecules and cyanides ($\text{OH}\cdots\text{NC}$) are presented as black dotted lines while the π - π interactions between 4-OHpy rings and cyanides are presented as red dotted lines. The respective distances in [\AA] are 2.88 and 2.67 for O3–N4 and O2–N5, respectively, while the average distance between centre of 4-OHpy ring and CN bond is ca. 3.5 \AA . Colours: Dy, brown; Co, dark green; C, light green; N, light blue; O, orange; hydrogen, light grey.

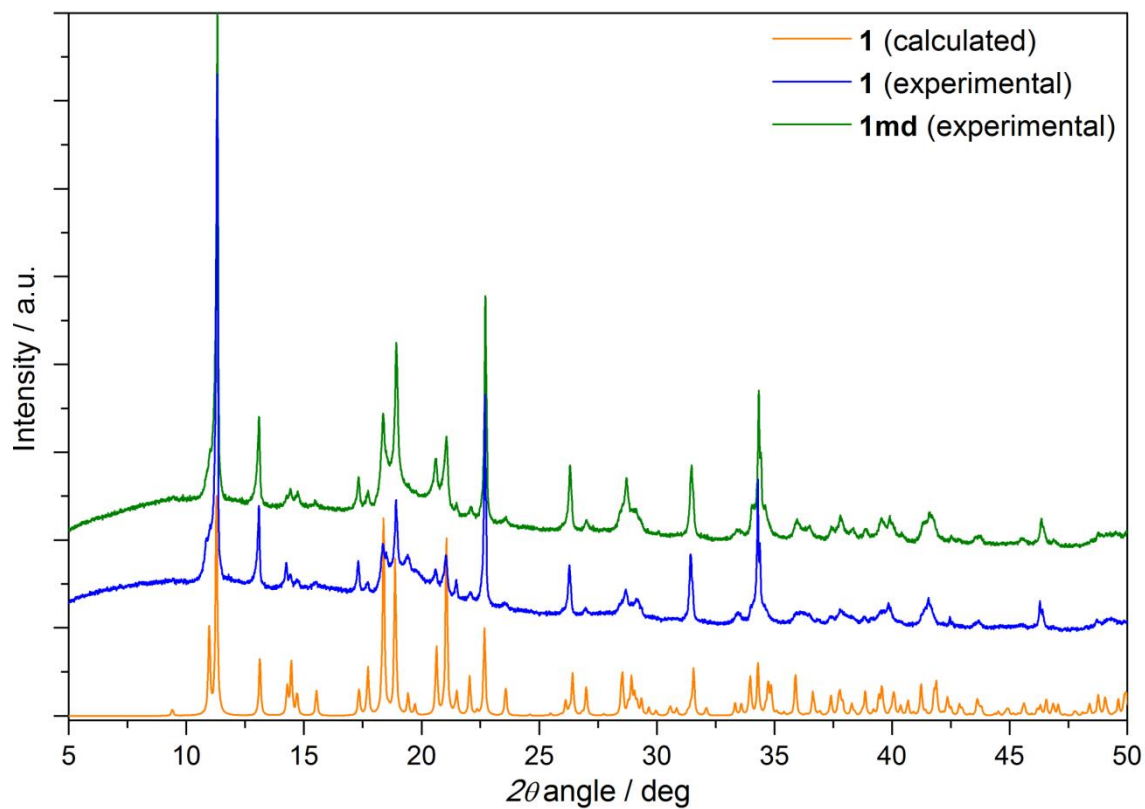


Figure S6. Experimental powder X-ray diffraction patterns of **1** (blue line), and its magnetically diluted sample, **1md** (green line), compared with the calculated pattern based on the single-crystal XRD structural model of **1** (orange line).

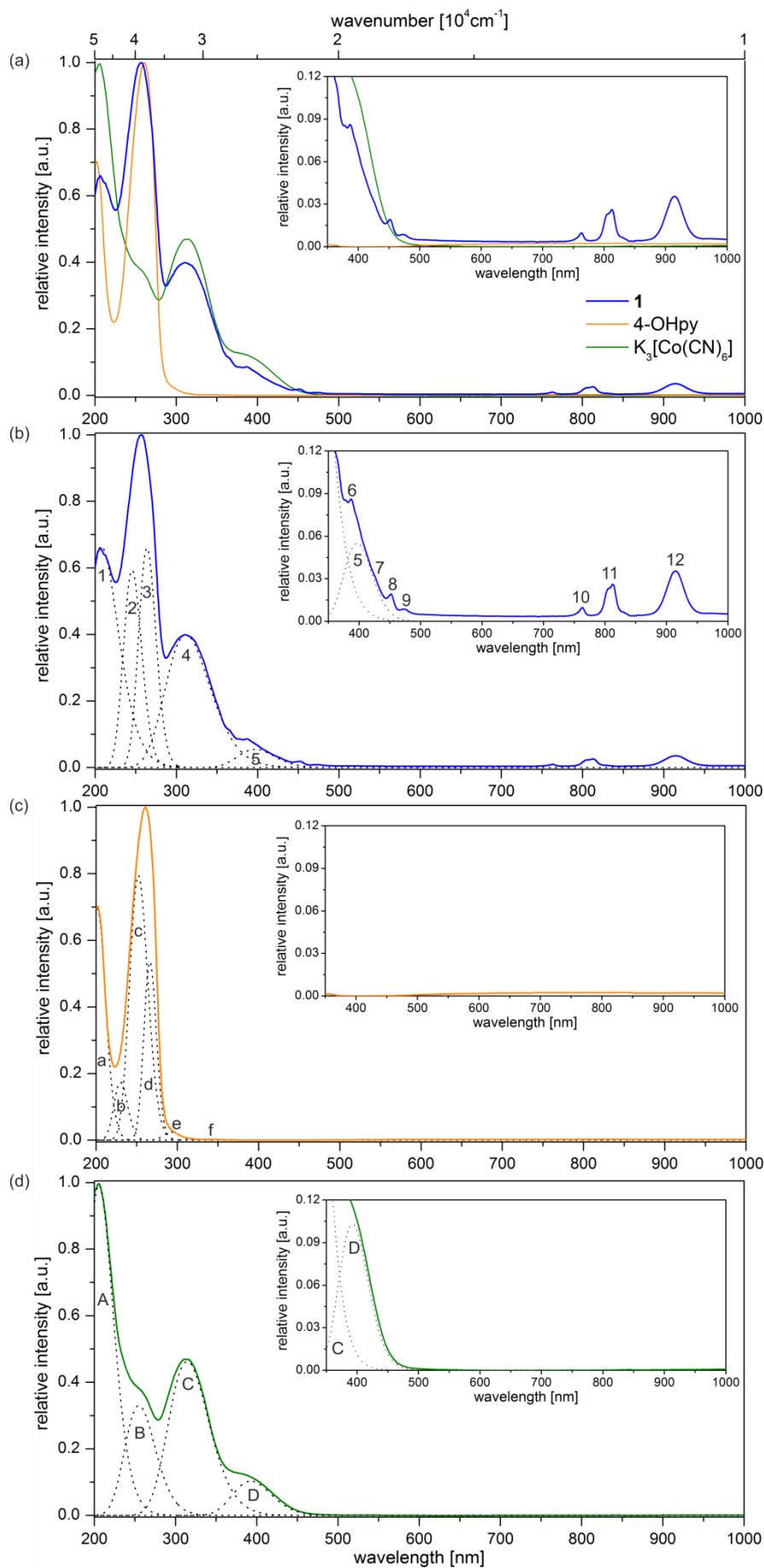


Figure S7. Solid state UV-Vis-NIR absorption spectra of **1** (a-b) compared with the spectra of 4-OHpy (c) and $K_3[Co(CN)_6]$ (d). Solid lines show the experimental data, dotted lines the deconvoluted components (see Table S7).

Table S4. Analysis of solid state UV-Vis-NIR absorption spectrum of **1** compared with the analyses of the relevant spectra of 4-OHpy and $K_3[Co^{III}(CN)_6]$ (see Figure S7).

compound (figure)	peak no.	λ_{max} [nm]	E_{max} [cm^{-1}]	interpretation
1	1	207	48200	combined contribution from d-d of Co^{III-LS} : $A_{1g} \rightarrow {}^1E_g$ and singlet to singlet transition of 4OH-py: $\pi \rightarrow \pi^*$
	2	245	40750	combined contribution from d-d of Co^{III-LS} : $A_{1g} \rightarrow {}^1T_{2g}$ and singlet to singlet transitions of 4OH-py: $\pi \rightarrow \pi^*$
	3	264	37930	singlet to singlet transition of 4OH-py: $\pi \rightarrow \pi^*$
	4	312	32100	combined contribution from d-d of Co^{III-LS} : $A_{1g} \rightarrow {}^1T_{1g}$ and singlet to triplet transition of 4OH-py: $\pi \rightarrow \pi^*$
	5	397	25200	combined contribution from d-d of Co^{III-LS} : $A_{1g} \rightarrow {}^3T_{1g}$ and singlet to triplet transition of 4OH-py: $\pi \rightarrow \pi^*$
	6	387	25840	f-f of $Dy^{III, [S4]}$: ${}^6H_{15/2} \rightarrow {}^4H_{13/2}$
	7	423	26460	f-f of Dy^{III} : ${}^6H_{15/2} \rightarrow {}^4G_{15/2}$
	8	452	22120	f-f of Dy^{III} : ${}^6H_{15/2} \rightarrow {}^4I_{15/2}$
	9	473	21140	f-f of Dy^{III} : ${}^6H_{15/2} \rightarrow {}^4F_{9/2}$
	10	763	13100	f-f of Dy^{III} : ${}^6H_{15/2} \rightarrow {}^6F_{3/2}$
	11	813	12300	f-f of Dy^{III} : ${}^6H_{15/2} \rightarrow {}^6F_{5/2}$
	12	915	10930	f-f of Dy^{III} : ${}^6H_{15/2} \rightarrow {}^6F_{7/2}$
4-OHpy	a	201	49640	singlet to singlet transitions: ^[S5] $\pi \rightarrow \pi^*$
	b	230	43500	
	c	252	39700	
	d	266	37570	
	e	292	34200	singlet to triplet transition: $\pi \rightarrow \pi^*$
	f	352	28410	
$K_3[Co(CN)_6]$	A	205	48700	d-d of $Co^{III-LS, [S1, S6]}$: ${}^1A_{1g} \rightarrow {}^1E_g$
	B	255	39240	d-d of Co^{III-LS} : ${}^1A_{1g} \rightarrow {}^1T_{2g}$ (minor contribution of ${}^1A_{1g} \rightarrow {}^5T_{2g}$)
	C	314	31830	d-d of Co^{III-LS} : ${}^1A_{1g} \rightarrow {}^1T_{1g}$ (minor contribution of ${}^1A_{1g} \rightarrow {}^3T_{2g}$)
	D	393	25470	d-d of Co^{III-LS} : ${}^1A_{1g} \rightarrow {}^3T_{1g}$

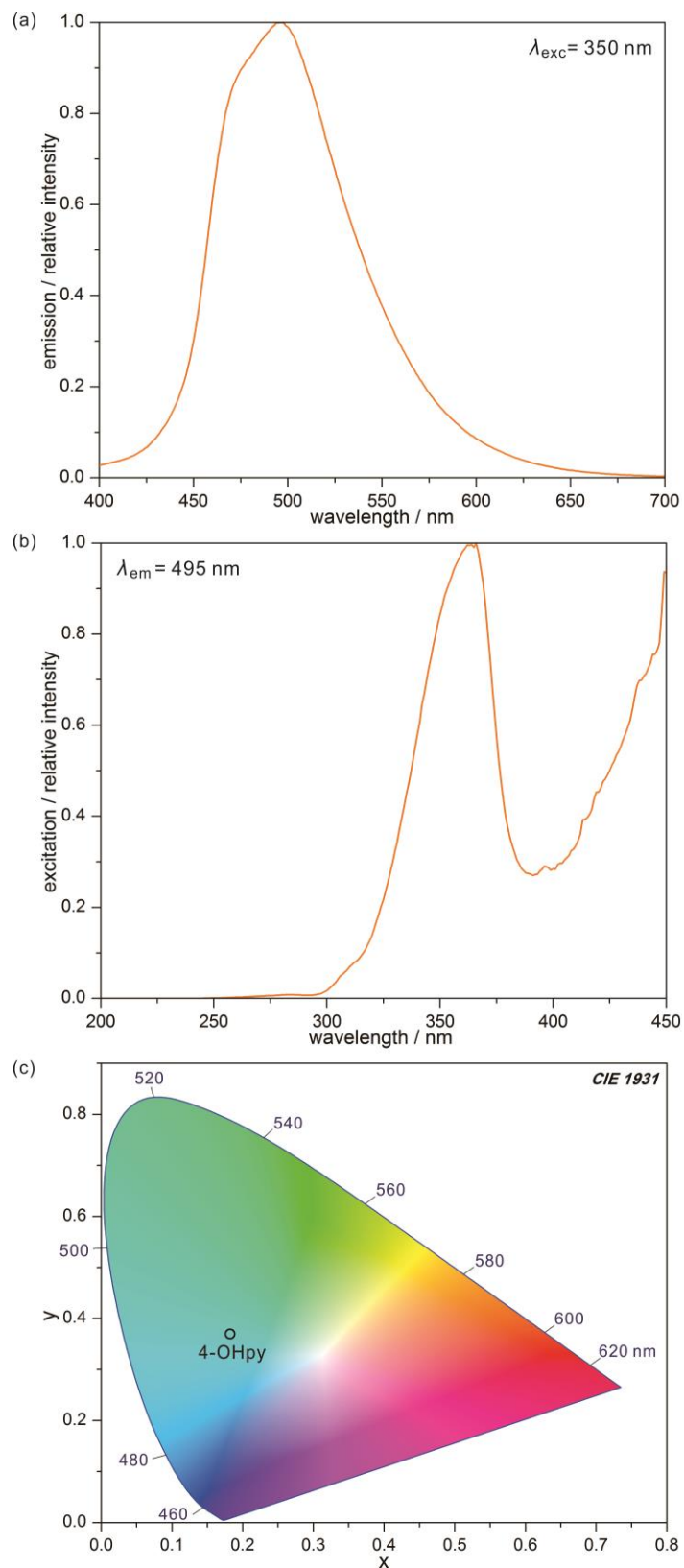


Figure S8. Solid state UV-Vis emission (a) and excitation (b) spectra of free 4-OHpy under the indicated conditions, together with the related emission colour presented on the CIE 1931 chromaticity diagram (c).

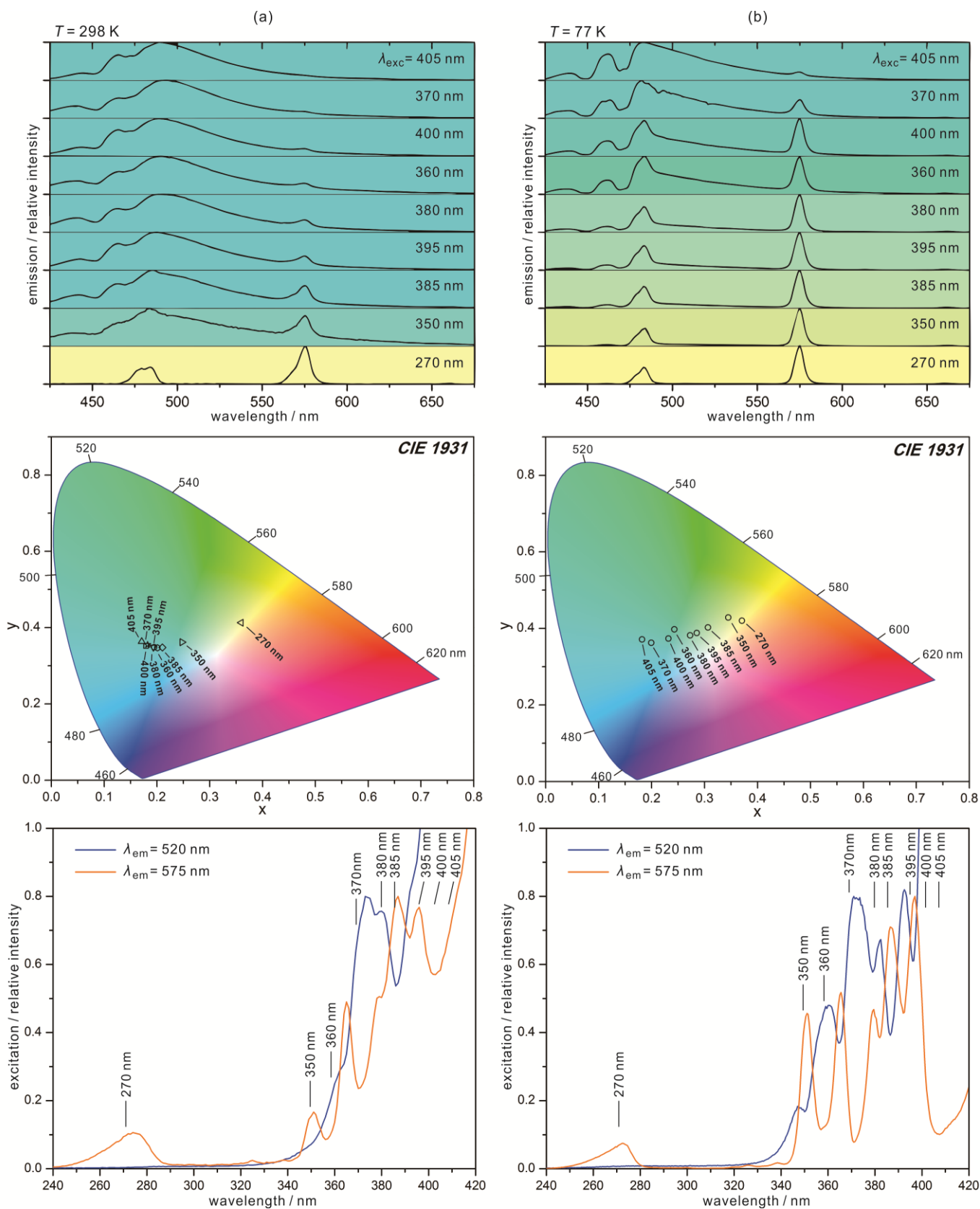


Figure S9. Room temperature (a, $T = 298\text{ K}$) and low temperature (b, $T = 77\text{ K}$) solid state UV-Vis emission spectra of **1** under various indicated excitation wavelengths (top part), together with the emission colours presented on the CIE 1931 chromaticity diagrams (middle part), and the related excitation spectra (bottom part) for the monitored emission peaks of 4-OHpy ($\lambda_{\text{em}} = 520\text{ nm}$) and Dy^{III} ($\lambda_{\text{em}} = 575\text{ nm}$).

Table S5. Summary of xy parameters of the CIE 1931 chromaticity scale for the emission colours of **1** detected at room and low temperature at various indicated wavelength of the excitation light (Figure S9).

$\lambda_{\text{exc}} / \text{nm}$	Room temperature ($T = 298 \text{ K}$)		Low temperature ($T = 77 \text{ K}$)	
	x	y	x	y
270	0.359	0.413	0.371	0.420
350	0.201	0.347	0.345	0.428
360	0.182	0.355	0.243	0.398
370	0.193	0.349	0.200	0.362
380	0.210	0.348	0.273	0.382
385	0.201	0.344	0.306	0.403
395	0.195	0.349	0.285	0.388
400	0.180	0.352	0.232	0.374
405	0.171	0.363	0.182	0.371

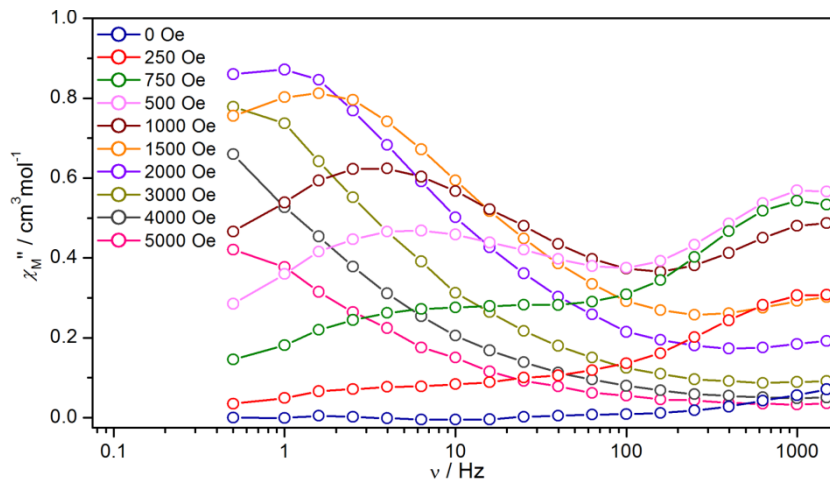


Figure S10. Frequency dependences of in-plane χ_M' and out-of-plane χ_M'' magnetic susceptibility of **1** under *ac* magnetic field of 3 Oe at $T = 1.9$ K, and indicated *dc* magnetic fields. Solid lines are added only to guide the eye.

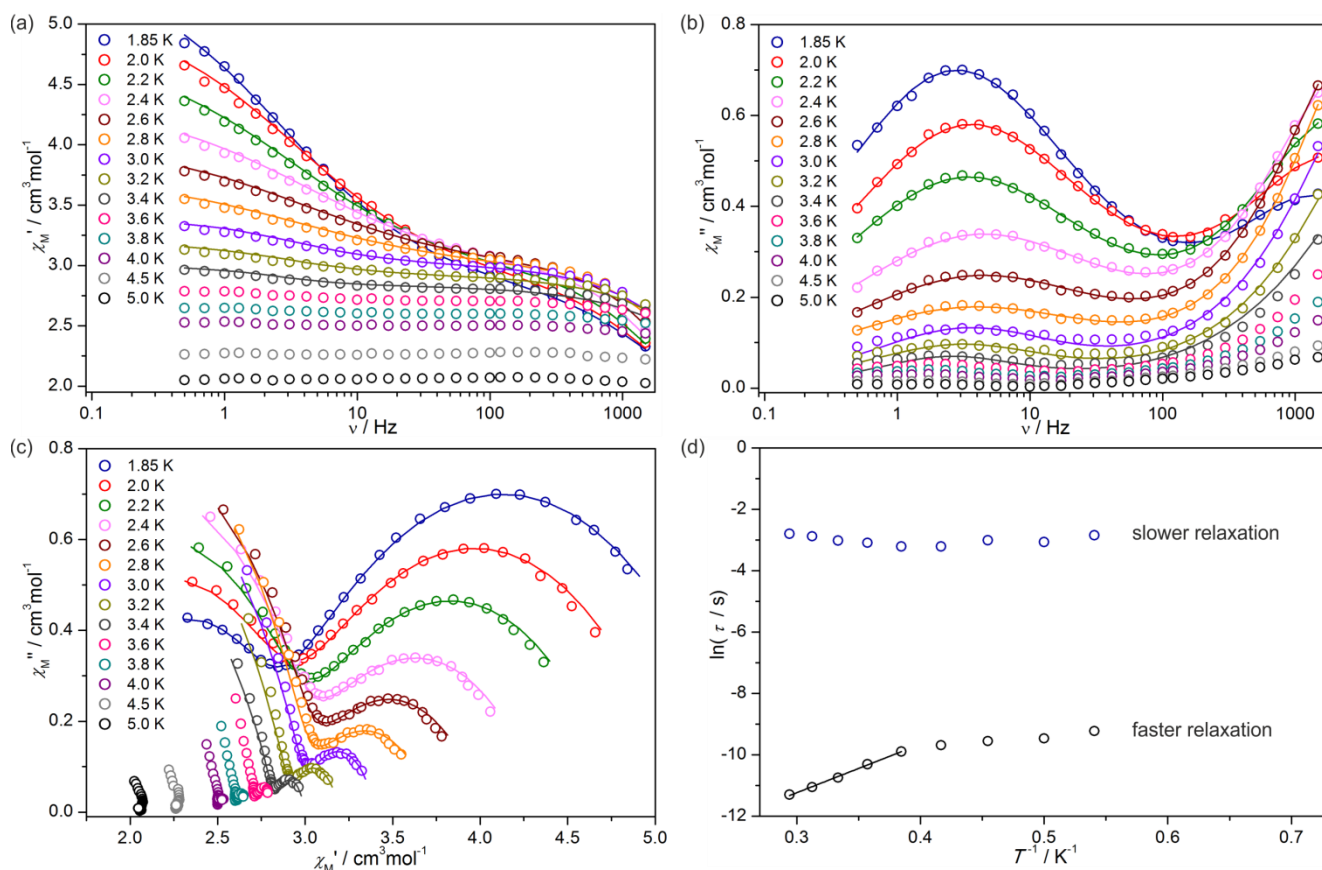


Figure S11. Full *ac* magnetic characteristics of **1** under $H_{dc} = 1000$ Oe and $H_{ac} = 3$ Oe: frequency (ν) dependences of the in-plane, χ_M' (a) and out-of-plane, χ_M'' (b) components of the complex magnetic susceptibility for the indicated temperatures of the 1.85–5.0 K range, the related χ_M'' – χ_M' Argand plots, and the temperature dependence of relaxation times (τ) presented as $\ln(\tau)$ versus T^{-1} plots. Solid lines in (a–c) were fitted using the generalized Debye model (Table S5), whereas the solid line in (d) are fitting to the Arrhenius law ($\ln\tau = \ln\tau_0 - (\Delta E/k_B) \cdot T^{-1}$), giving the energy barrier, $\Delta E/k_B = 15.8(5)$ K, and the pre-exponential factor, $\tau_0 = 1.2(3) \cdot 10^{-7}$ s.

Table S6. Parameters obtained by fitting the Argand $\chi_M''-\chi_M'$ plots ($H_{dc} = 1000$ Oe, Figure S11) of **1** using the generalized Debye model.

T / K	$\chi_{S,\text{total}}^{\text{cm}^3 \text{mol}^{-1}}$	$\Delta\chi_1^{\text{cm}^3 \text{mol}^{-1}}$	τ_1 / s	α_1	$\Delta\chi_2^{\text{cm}^3 \text{mol}^{-1}}$	τ_2 / s	α_2
1.85	1.72	2.79	0.0582	0.411	1.03	0.0000985	0.204
2.0	1.46	2.33	0.0467	0.419	1.38	0.0000775	0.241
2.2	1.35	1.90	0.0494	0.430	1.56	0.0000711	0.205
2.4	1.22	1.43	0.0394	0.446	1.72	0.0000621	0.164
2.6	1.08	1.06	0.0403	0.452	1.89	0.0000504	0.149
2.8	0.776	0.760	0.0454	0.453	2.20	0.0000335	0.163
3.0	0.568	0.393	0.0491	0.271	2.43	0.0000215	0.243
3.2	0.604	0.278	0.0562	0.255	2.32	0.0000158	0.253
3.4	0.710	0.260	0.0606	0.256	2.25	0.0000124	0.303

The following equations of the generalized Debye model for two relaxation processes were applied:

$$\chi'(\omega) = \chi_{S,\text{total}} + \Delta\chi_1 \frac{1 + (\omega\tau_1)^{1-\alpha_1} \sin(\pi\alpha_1/2)}{1 + 2(\omega\tau_1)^{1-\alpha_1} \sin(\pi\alpha_1/2) + (\omega\tau_1)^{2(1-\alpha_1)}} + \Delta\chi_2 \frac{1 + (\omega\tau_2)^{1-\alpha_2} \sin(\pi\alpha_2/2)}{1 + 2(\omega\tau_2)^{1-\alpha_2} \sin(\pi\alpha_2/2) + (\omega\tau_2)^{2(1-\alpha_2)}}$$

$$\chi''(\omega) = \Delta\chi_1 \frac{(\omega\tau_1)^{1-\alpha_1} \cos(\pi\alpha_1/2)}{1 + 2(\omega\tau_1)^{1-\alpha_1} \sin(\pi\alpha_1/2) + (\omega\tau_1)^{2(1-\alpha_1)}} + \Delta\chi_2 \frac{(\omega\tau_2)^{1-\alpha_2} \cos(\pi\alpha_2/2)}{1 + 2(\omega\tau_2)^{1-\alpha_2} \sin(\pi\alpha_2/2) + (\omega\tau_2)^{2(1-\alpha_2)}}$$

where

$\chi_{S,\text{total}}$ = the sum of the adiabatic susceptibility of two relaxation processes ($\chi_{S,1} + \chi_{S,2}$),

$\Delta\chi_1$ = the difference between the adiabatic susceptibility ($\chi_{S,1}$) and the isothermal susceptibility ($\chi_{T,1}$) of the first relaxation process,

$\Delta\chi_2$ = the difference between the adiabatic susceptibility ($\chi_{S,2}$) and the isothermal susceptibility ($\chi_{T,2}$) of the second relaxation process,

τ_1 and τ_2 = the relaxation times of the first and the second relaxation processes, respectively,

α_1 and α_2 = the distribution (Cole-Cole) parameters of the first and the second relaxation processes, respectively,

and ω is an angular frequency, that is $\omega = 2\pi\nu$, with ν stands for the linear frequency in [Hz] units.^[S7]

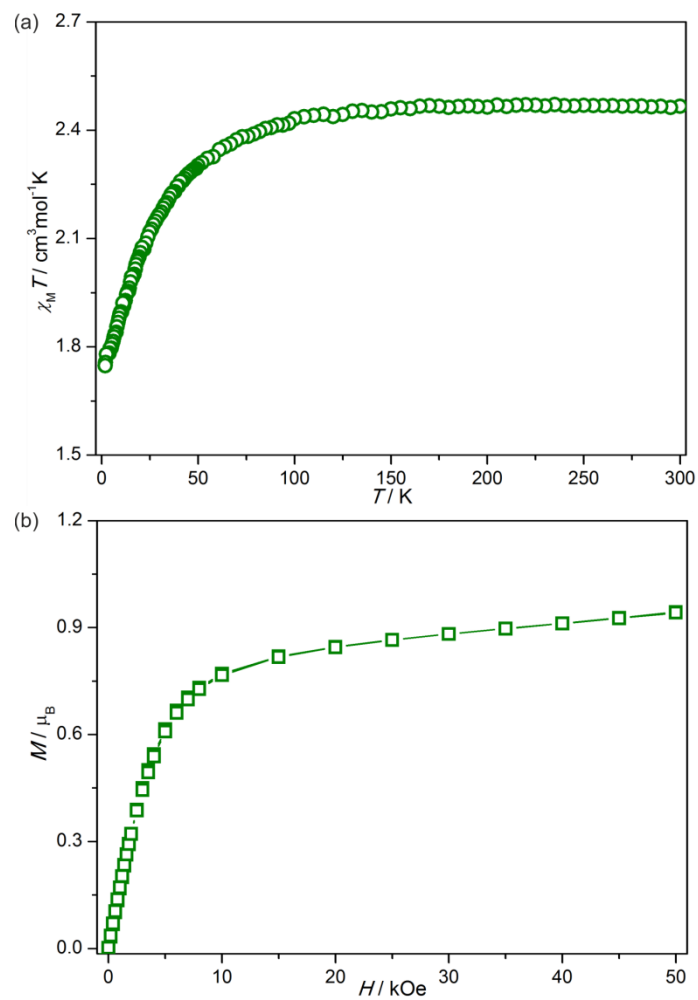


Figure S12. Direct-current (*dc*) magnetic properties of **1md**: temperature dependence of $\chi_M T$ at $H_{\text{dc}} = 1000$ Oe (a), and the field dependence of molar magnetization, M at $T = 1.8$ K (b).

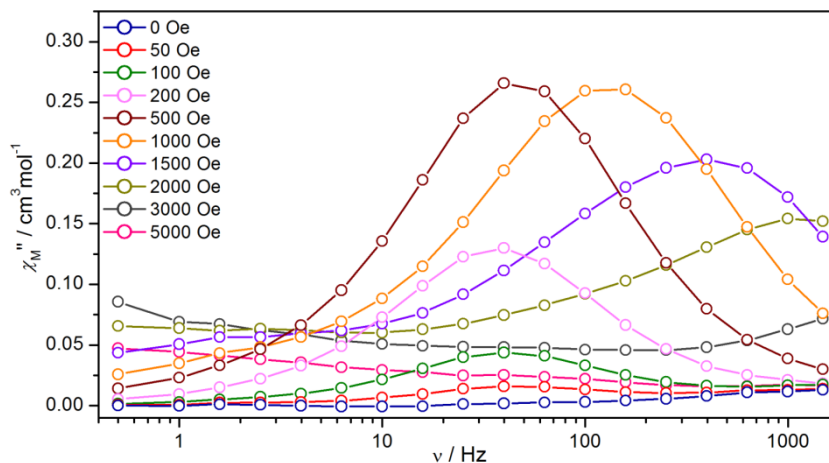


Figure S13. Frequency dependences of in-plane χ_M' and out-of-plane χ_M'' magnetic susceptibility of **1md** under *ac* magnetic field of 3 Oe at $T = 1.9$ K, and indicated *dc* magnetic fields. Solid lines are added only to guide the eye.

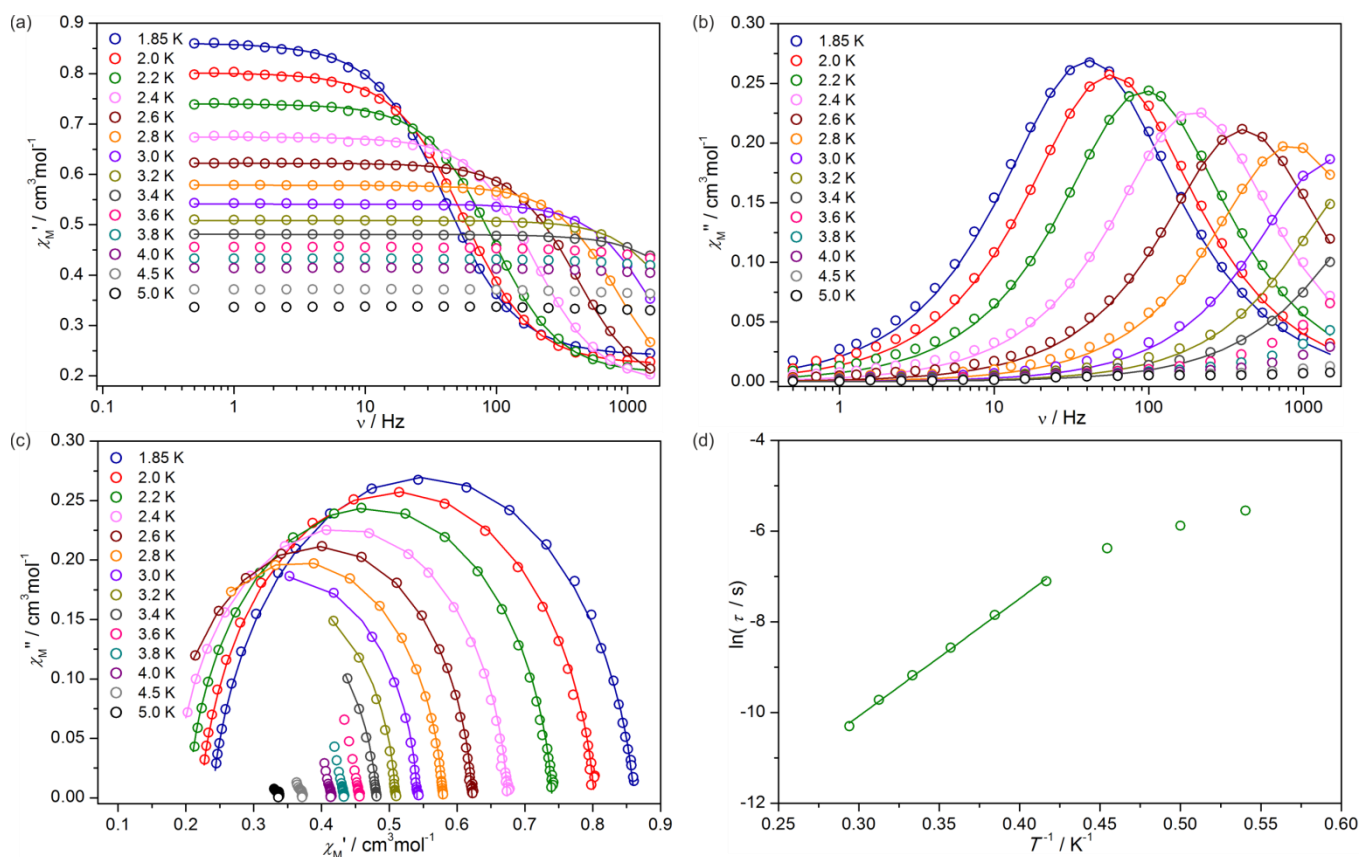


Figure S14. Full *ac* magnetic characteristics of **1md** under $H_{dc} = 500$ Oe and $H_{ac} = 3$ Oe: frequency (ν) dependences of the in-plane, χ_M' (a) and out-of-plane, χ_M'' (b) components of the complex magnetic susceptibility for the indicated temperatures of the 1.85–5.0 K range, the related χ_M'' – χ_M' Argand plots, and the temperature dependence of relaxation times (τ) presented as $\ln(\tau)$ versus T^{-1} plots. Solid lines in (a–c) were fitted using the generalized Debye model (Table S5), whereas the solid line in (d) are fitting to the Arrhenius law ($\ln\tau = \ln\tau_0 - (\Delta E/k_B) \cdot T^{-1}$), giving the energy barrier, $\Delta E/k_B = 25.9(6)$ K, and the pre-exponential factor, $\tau_0 = 1.8(4) \cdot 10^{-8}$ s.

Table S7. Parameters obtained by fitting the Argand χ_M'' - χ_M' plots ($H_{dc} = 500$ Oe, Figure S14) of **1md** using the generalized Debye model.

T / K	χ_S $\text{cm}^3 \text{mol}^{-1}$	χ_T $\text{cm}^3 \text{mol}^{-1}$	τ / s	α
1.85	0.239	0.861	0.00390	0.0910
2.0	0.222	0.802	0.00281	0.0763
2.2	0.204	0.740	0.00174	0.0604
2.4	0.185	0.674	0.000819	0.0484
2.6	0.169	0.622	0.000390	0.0441
2.8	0.152	0.578	0.000193	0.0460
3.0	0.148	0.541	0.000103	0.0349
3.2	0.143	0.508	0.0000603	0.0331
3.4	0.120	0.481	0.0000337	0.0647

The following equations of the generalized Debye model for single relaxation process were applied:

$$\chi'(\omega) = \chi_S + (\chi_T - \chi_S) \frac{1 + (\omega\tau)^{1-\alpha} \sin(\pi\alpha/2)}{1 + 2(\omega\tau)^{1-\alpha} \sin(\pi\alpha/2) + (\omega\tau)^{2(1-\alpha)}}$$

$$\chi''(\omega) = (\chi_T - \chi_S) \frac{(\omega\tau)^{1-\alpha} \cos(\pi\alpha/2)}{1 + 2(\omega\tau)^{1-\alpha} \sin(\pi\alpha/2) + (\omega\tau)^{2(1-\alpha)}}$$

where

χ_S = the adiabatic susceptibility (at infinitely high frequency of ac field),

χ_T = the isothermal susceptibility (at infinitely low frequency of ac field),

τ = the relaxation time,

α = the distribution (Cole-Cole) parameter,

and ω is an angular frequency, that is $\omega = 2\pi\nu$, with ν stands for the linear frequency in [Hz] units.^[S7]

References to Supporting Information

- [S1] S. Chorazy, M. Rams, K. Nakabayashi, B. Sieklucka and S. Ohkoshi, *Chem. Eur. J.*, 2016, **22**, 7371.
- [S2] G. M. Sheldrick, *Acta Crystallogr.*, 2008, **A64**, 112.
- [S3] (a) M. Llunell, D. Casanova, J. Cirera, J. Bofill, P. Alemany, S. Alvarez, M. Pinsky, D. Avnir, *SHAPE v. 2.1. Program for the Calculation of Continuous Shape Measures of Polygonal and Polyhedral Molecular Fragments*, University of Barcelona: Barcelona, Spain, 2013; (b) D. Casanova, J. Cirera, M. Llunell, P. Alemany, D. Avnir and S. Alvarez, *J. Am. Chem. Soc.*, 2004, **126**, 1755.
- [S4] (a) J. Feng, H.-J. Zhang, S.-Y. Song, Z.-F. Li, L.-N. Sun, Y. Xing and X.-M. Guo, *J. Lumin.*, 2008, **128**, 1957; (b) J. Feng, L. Zhou, S.-Y. Song, Z.-F. Li, W.-Q. Fan, L.-N. Sun, Y.-N. Yu and H.-J. Zhang, *Dalton Trans.*, 2009, 6593; (c) G. Kaur and S. B. Rai, *J. Fluoresc.*, 2012, **22**, 475; (d) E. Pavitra, G. Seeta Rama Raju, W. Park and J. Su Yu, *New J. Chem.*, 2014, **38**, 163; (e) D. D. Ramteke and R. S. Gedam, *Spectr. Lett.*, 2015, **48**, 417.
- [S5] (a) A. Weisstuch, P. Neidig and A. C. Testa, *J. Lumin.*, 1975, **10**, 137; (b) P. Beak, F. S. Fry, J. Lee and F. Steele, *J. Am. Chem. Soc.*, 1976, **98**, 171; (c) S. Hotchandani and A. C. Testa, *J. Chem. Phys.*, 1977, **67**, 5201.
- [S6] (a) V. M. Miskowski, H. B. Gray, R. B. Wilson and E. I. Solomon, *Inorg. Chem.*, 1979, **18**, 1410; (b) H. Kunkely and A. Vogler, *Inorg. Chem. Commun.*, 2004, **7**, 770; (c) T. Lazarides, G. M. Davies, H. Adams, C. Sabatini, F. Barigelletti, A. Barbieri, S. J. A. Pope, S. Faulkner and M. D. Ward, *Photochem. Photobiol. Sci.*, 2007, **6**, 1152.
- [S7] (a) Y.-N. Guo, G.-F. Xu, Y. Guo and J. Tang, *Dalton Trans.* 2011, **40**, 9953; (b) M. Ramos Silva, P. Martin-Ramos, J. T. Coutinho, L. C. J. Pereira and J. Martin-Gil, *Dalton Trans.* 2014, **43**, 6752.